No Evidence of Phase-Amplitude Coupling in Auditory Steady-State Responses

Aurimas Mockevičius and Inga Griškova-Bulanova

***Abstract*— Phase-amplitude coupling (PAC), reflecting the modulation of high-frequency amplitude by the phase of lower-frequency oscillations, is increasingly recognized as a key mechanism underlying neural information processing. While PAC is typically associated with higher-order perceptual and cognitive processes, some studies explored PAC in relation to auditory steady-state responses (ASSR), a paradigm commonly used to assess gamma-band synchronization. However, findings from these studies remain inconclusive due to methodological variability and challenges in PAC analysis. In this study, we systematically investigated PAC in the EEG signal recorded during 40 Hz auditory steady-state stimulation using a rigorous analysis pipeline with three established PAC estimation methods: Mean Vector Length, Kullback-Leibler Modulation Index, and Phase-Locking Value. Our approach was validated on simulated EEG-like signals and applied to scalp EEG data from 12 participants (26.7 ± 3.6 years, 5 females) in 40 Hz ASSR and resting-state (rsEEG) conditions. We found no significant differences in PAC between ASSR and rsEEG conditions in the ASSR-associated fronto-central region, regardless of PAC estimation methods. Furthermore, individual-specific peak PAC values and their associated frequencies showed no consistent patterns across conditions. These results suggest that PAC is not reliably elicited by auditory steady-state stimulation in EEG, challenging the utility of the ASSR paradigm for assessing PAC.**

***Index Terms*— Auditory steady-state response, cross-frequency coupling, electroencephalogram, phase-amplitude coupling.**

I. Introduction

SYNCHRONIZED neural activity is fundamental for neural information processing [1]. It is reflected by a measurable oscillatory signal obtained using electro- (EEG) or magnetoencephalography (MEG). Typically, the activity of different frequency bands within the signal is analyzed, i. e. delta (1-4 Hz), theta (5-8 Hz), alpha (9-12 Hz), beta (13-30 Hz) and gamma (>30 Hz), which are associated with a variety of functional aspects [2], [3], [4]. However, accumulating evidence points to the importance of cross-frequency interactions in neural processing [5], [6], [7]. In particular, studies focus on phase-amplitude coupling (PAC) which reflects the modulation of high frequency amplitude by the phase of low frequency activity [8], [9]. It is thought that PAC represents the interaction between neural processes occurring at different spatiotemporal scales that facilitates neural communication [10], being detected in visual and auditory tasks [11], [12], [13], [14], [15] as well as in resting-state conditions [16], [17]. Importantly, PAC alterations are evident in neuropsychiatric disorders [18], [19], [20], where an increasing interest in identifying reliable markers of brain activity dynamics is observed.

One particularly promising measure reflecting state of brain networks is the auditory steady-state response (ASSR). ASSR, an oscillatory neural response, especially prominent at gamma frequencies, is evoked by periodic auditory stimulation [21] and shows high test-retest reliability [22], [23] and temporal stability [24]. It is consistently altered in neuropsychiatric disorders [25], [26], [27] and is associated with certain aspects of information processing [28] and attention levels [29]. Several studies analyzed PAC during gamma-range auditory steady-state stimulation expecting that the evoked response could reflect cross-frequency interactions [30]. It was shown that PAC during auditory periodic stimulation may differ between clinical groups and healthy controls [31], [32], [33], [34] or between experimental conditions [35], [36], making it a promising measure. In addition, higher PAC in response to auditory periodic stimuli as compared to the baseline activity has been observed [33], [34], [37], providing preliminary evidence that ASSR paradigm could indeed be used for PAC assessment.

However, many studies suggest that PAC analysis using traditional estimation methods is highly susceptible to various confounding factors that can result in spurious PAC, including data length [38], filtering bandwidths [39], signal-to-noise ratio [40], edge artifacts [41], non-sinusoidal oscillations [42] and non-stationary activity [39]. The confounders can be mitigated by selecting proper analysis parameters and/or using control procedures. In a recent review, we performed a systematic evaluation of PAC analysis approaches used in ASSR-PAC

Received 3 July 2025; revised 26 November 2025 and 25 January 2026; accepted 17 March 2026. Date of publication 23 March 2026; date of current version 1 April 2026. Associate Editor: Fani Deligianni. This work was supported by the Research Council of Lithuania (LMTLT) under Agreement S-LJB-20-1. *(Corresponding author: Inga Griškova-Bulanova.)*

This work involved human subjects or animals in its research. Approval of all ethical and experimental procedures and protocols was granted by Vilnius Regional Biomedical Research Ethics Committee under Application No. 2020/3-1213-701.

Aurimas Mockevičius is with the Translational Health Research Institute, Medical Science Center, Vilnius University, Vilnius LT-01513, Lithuania (e-mail: aurimas.mockevicius@mf.vu.lt).

Inga Griškova-Bulanova is with the Translational Health Research Institute, Medical Science Center, and the Institute of Biosciences, Life Sciences Center, Vilnius University, Vilnius LT-01513, Lithuania (e-mail: inga.griskova-bulanova@gf.vu.lt).

This article has supplementary downloadable material available at https://doi.org/10.1109/TNSRE.2026.3676768, provided by the authors.

Digital Object Identifier 10.1109/TNSRE.2026.3676768

TABLE I
CONFOUNDING FACTORS RELEVANT TO PAC ESTIMATION AND MEASURES APPLIED TO CONTROL THEM IN THE PRESENT STUDY

Confounding factor	Measures
Frequency bandwidth [39]	Narrow (±1 Hz) bandwidth for phase, broad (± upper sideband of phase frequency) for amplitude
Data length [38], [40]	Sufficiently long analyzed time window (1500 ms)
Signal-to-noise ratio [40]	Sufficiently long analyzed time window (1500 ms); Surrogate normalization
Edge artifacts [41]	Filtering before epoching; exclusion of epoch edges after Hilbert transform
Non-stationary periods [39]	Excluded stimulus onset activity (0-500 ms)
Non-sinusoidal oscillations [42]	Surrogate normalization
PAC output dependence on estimation method [38]	Application of different PAC estimation methods for the same data

studies [30] and showed profound differences among the studies in terms of findings and the applied methodological procedures.

Previous ASSR-PAC studies also varied considerably in the extent to which confounding factors were addressed, with a number of studies being particularly susceptible to the potential of artifactual coupling [30], overall suggesting that the available evidence for ASSR-related PAC is still limited and may not be sufficiently reliable. Therefore, in the present work, we sought to address the limitations of the previous studies by setting up an analysis pipeline which addressed PAC analysis-related problematic aspects in order to evaluate the presence of PAC in 40 Hz ASSRs. The list of confounds that were addressed in the analysis pipeline is adapted based on our previous review [30]. These are summarized in Table I.

To address the issues in the existing ASSR-PAC literature, we used a realistic simulated signal with implemented PAC to validate our approach and further applied the pipeline to the real EEG data, aiming to evaluate ASSR-related PAC by comparing auditory steady-state stimulation condition with the resting-state, which is characterized by the absence of periodic gamma activity [43]. The main goal of this study is to investigate whether ASSR paradigm, often employed for the evaluation of gamma synchronization in the context of neuropsychiatric disorders [25], [26], [27] and non-invasive neuromodulation [44], [45], could also be used for PAC assessment.

II. METHODS

A. Subjects

13 volunteers participated in the experiment. Each participant had a hearing threshold within the normal range (<25 dB). Data from 1 subject were excluded due to excessively noisy recordings, resulting in a sample of 12 healthy participants (26.7 ± 3.6 years, 5 females). Participants were university students, all right-handed. All participants gave written informed consent, and bioethical approval was granted for the study by Vilnius Regional Biomedical Research Ethics Committee (no. 2020/3-1213-701).

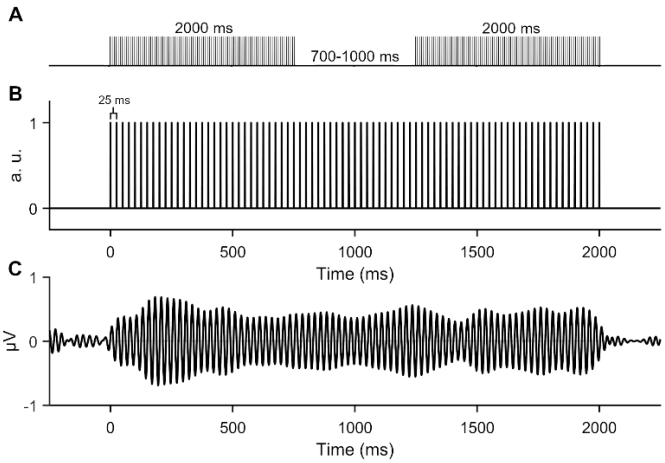

Fig. 1. Stimulation sequence (A), schematic representation of a 40-Hz click stimulus (B) and a corresponding trial-averaged single-subject 40-Hz response.

B. EEG Data

At the beginning of the experiment, 5-min eyes-closed resting-state EEG (rsEEG) activity was recorded, followed by ASSR paradigm. Auditory stimulation consisted of 2000-ms click trains (Figure 1). Stimuli were composed of equally spaced (25-ms) white noise clicks of 1.5 ms duration, corresponding to 40 Hz. Stimuli were repeated 75 times per block with a variable 700-1000 ms inter stimulus interval (ISI), two blocks were delivered in total resulting in 150 presentations. Participants listened to the sounds with their eyes closed. EEG was acquired using ANT device (ANT neuro, The Netherlands) with 64 channel WaveGuard EEG electrode (Ag/AgCl) cap with international 10-10 montage. Mastoids were used as a recording reference and ground electrode was attached close to Fz. Impedance was kept below 20 kΩ. Sampling rate was set at 2048 Hz.

Raw EEG data were preprocessed using EEGlab [46] in Matlab (R2020a) environment. A 1-100 Hz FIR filter was applied and CleanLine plugin was used to suppress 50-Hz line noise. Empty or excessively noisy electrodes were removed and recreated using spline interpolation. Data was re-referenced to the average of all EEG channels. Infomax independent component analysis as implemented in EEGlab script *runica* was computed and components related to eye movements were manually excluded by the visual inspection of component topographies and time series. On average, 2.81 ± 0.71 (2-4) components were removed. Segments with remaining noise or artifacts were manually removed. Data was downsampled to 1000 Hz.

C. Simulated Data

To simulate EEG-like data, Brownian noise was generated as suggested by [38], using scripts provided by [47]. The sampling rate was set at 1000 Hz. To introduce PAC into the signal, low-frequency activity (2 Hz, 6 Hz or 10 Hz) was filtered from the Brownian noise using zero-phase FIR filter implemented in EEGLab [46]. From the filtered signal, phase information was extracted via Hilbert transform and the cosine of the phase information was computed to recreate the original

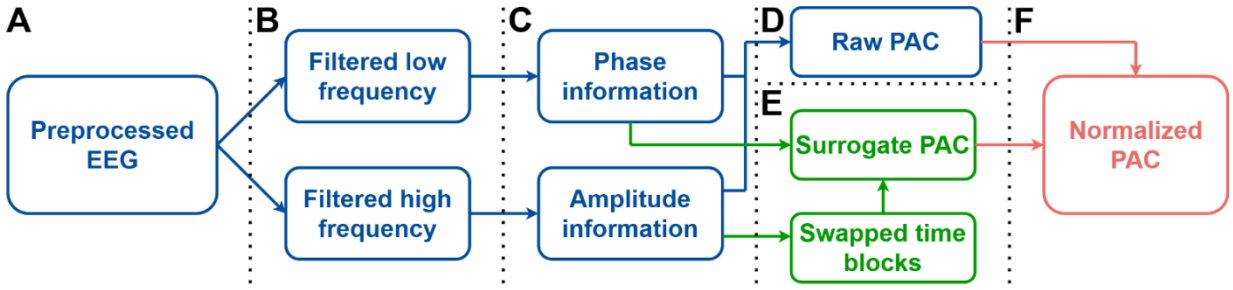

Fig. 2. Flowchart of analysis pipeline. Blue color indicates the sequence of raw PAC estimation; green color represents steps in surrogate PAC computation and red color shows the main output–normalized PAC. A. Preprocessed EEG data were used for analysis. B. For each PAC phase-amplitude frequency pair, data were filtered into separate low-frequency (phase) and high-frequency (amplitude) time series. C. After epoching the filtered signals, phase and amplitude information was extracted from low-frequency and high-frequency time series, respectively. D. Raw PAC was computed using MVL-MI, KL-MI and PLV-MI methods. E. Amplitude envelope of the high-frequency signal was cut at a random time point and the time blocks were swapped; unchanged phase information and the swapped amplitude envelope were used for surrogate PAC estimation. F. Raw PAC was normalized using surrogate PAC to obtain the z score.

low-frequency signal with constant amplitude. Then, 40-Hz sine was generated and further amplitude-modulated using the extracted low-frequency signal. The amplitude of the modulated 40-Hz signal was adjusted by multiplying its amplitude by the ratio of 40-Hz activity power between the Brownian noise signal and the modulated signal. Then, the modulated signal was added to the Brownian noise signal. The final output contained the 1/f characteristic typical of the EEG aperiodic activity and a periodic 40-Hz component with its amplitude coupled to the phase of the low-frequency activity already present in the Brownian noise signal. Three PAC signals were generated, in which 40-Hz amplitude was coupled to the phase of 2 Hz (delta), 6 Hz (theta) or 10 Hz (alpha). In addition, no-PAC signal with a pure-sine 40-Hz component added to the Brownian noise signal was simulated. The Matlab code for signal simulation is provided in Supplementary material S1.

D. Data Analysis

Data analysis consisted of two stages. First, responses to auditory stimulation were analyzed by conventional means to ensure that ASSR was evoked by the stimuli. Second, PAC estimation followed on ASSR, rsEEG and simulated data.

Time-frequency analysis. First, continuous data were epoched at -500 to 2500 ms relative to stimulus onset time. Time frequency analysis was performed using Fieldtrip [48]. Morlet wavelet transform was applied to the frequency range of 2-50 Hz in 1 Hz step using variable cycle length (2 for 2-3 Hz, 3 for 4-8 Hz, 5 for 9-15 Hz and 7 for the remaining frequencies). Both amplitude and phase information were extracted to compute the amplitude averaged over trials and phase-locking index (PLI, phase consistency over trials). Relative baseline normalization was applied to both measures, based on the average values in the time window of -500 ms to 0 ms relative to stimulus onset.

Phase-amplitude coupling. The flowchart of PAC analysis pipeline is schematically depicted in Figure 2. The extraction of phase and amplitude information was performed for multiple phase and amplitude frequency pairs. First, continuous data were filtered into separate low-frequency and high-frequency time series by applying zero-phase FIR filter implemented in EEGLab (Figure 2B). 2-12 Hz frequencies in 1 Hz step with a narrow ± 1 Hz bandwidth were selected for phase frequencies. For amplitude frequencies, 20-100 Hz in 2 Hz step were filtered, using a variable bandwidth which was equal to the upper sideband of the corresponding phase frequency [39]. For example, if the phase frequency was 8 Hz, then the bandwidth would be 7-9 Hz; if the amplitude frequency was 40 Hz, then the bandwidth would be 31-49 Hz.

Filtered phase and amplitude time series were epoched. The continuous simulated signal was segmented into 100 epochs of 3500-ms duration. ASSR and rsEEG data were divided into overlapping 3500-ms epochs so that epoch edges can be later excluded. Hilbert transform was performed for the epoched data to obtain phase and amplitude information from the low-frequency and high-frequency time series, respectively (Figure 2C).

In EEG data, random 100 epochs were chosen for each subject to keep an equal number of epochs. 1500-ms time windows for PAC computation were selected, excluding the first and the last 1000 ms in each epoch. In ASSR data, the window for analysis was set between 500 ms to 2000 ms, relative to the stimulus onset. This approach ensured that the following PAC confounders were controlled: (1) stimulus onset in ASSR data characterized by correlated activity between frequency bands [39] and (2) potential edge artifacts [41] that could appear due to FIR filter and Hilbert transform; (3) impact of noise in PAC computation, which can be mitigated by keeping substantial data length by ensuring a higher number of low-frequency cycles in the analyzed time window [40].

Amplitude information of the high-frequency time series was min-max normalized as suggested by [33], resulting in the amplitude in each epoch ranging between 0 and 1. This way, (1) trial-wise and inter-subject variations in amplitude were minimized; (2) the amplitude ranges from simulated data and EEG data were equalized; (3) the temporal pattern of amplitude envelope which is essential for PAC was kept intact.

For PAC analysis (Figure 2D), Matlab-based scripts from [49] were adapted and are presented in Supplementary material S1. PAC was computed for 9 frontocentral electrodes (F1, Fz, F2, FC1, FCz, FC2, C1, Cz, C2) where PAC has been analyzed at sensor level in previous ASSR studies [30], and for each filtered phase (2-12 Hz) and amplitude (20-100 Hz) frequency pair. Three algorithms were

applied–mean vector length modulation index (MVL-MI, [8]), Kullbeck-Leiber modulation index (KL-MI, [9]), and phase-locking value modulation index (PLV-MI, [50]). These methods were selected given that (1) they are among the most commonly used PAC estimation approaches, (2) are based on different mathematical principles and (3) show different sensitivity to confounding factors [38]. MVL-MI combines phase and amplitude information to create a complex-valued signal where each vector corresponds to a single time point. The average vector represents coupling strength: uniform vector distribution would lead to a low coupling value, whereas highly clustered vectors would result in a strong coupling. In KL-MI approach, phase time-series are divided into phase bins (18 bins in the present work) and the mean amplitude within each phase bin is computed and normalized by the average value across all bins. Coupling strength is then estimated by comparing the amplitude-phase distribution with a uniform distribution via the Kullbeck-Leiber distance. When applying PLV-MI, the phase information of the amplitude envelope is obtained using the Hilbert transform. The coupling strength is then quantified by calculating a phase-locking value between the low frequency phase and the phase of the amplitude envelope.

Finally, surrogate normalization was applied (Figure 2E), which generally helps to exclude spurious PAC arising due to confounders and highlight the real coupling [51]. For each phase and amplitude frequency pair, 1000 permutations were performed in which amplitude time series of a randomly selected epoch were cut at a random time point and the time blocks were swapped, aiming to eliminate the phase-amplitude relationship while keeping other signal characteristics intact [39]. Then, PAC was computed for the shuffled time series using the same PAC algorithms. This way, a null distribution of PAC values of the shuffled data were generated. To highlight the real coupling, raw PAC of each frequency pair was normalized by computing the z score (Figure 2F), where the mean of the surrogate distribution is subtracted from the raw PAC value and divided by the standard deviation of the surrogate PAC values.

E. Statistical Analysis

Achieved statistical power was estimated using G*power software [52]. Post-hoc power analysis for dependent samples t-test yielded the achieved power of 0.83 for |d| = 0.8, 0.49 for |d| = 0.5 and 0.16 for |d| = 0.2. The current study was powered to detect high effect sizes as observed in previous ASSR-PAC studies which compared stimulation and resting periods [33], [34], [37]. Statistical analysis was carried out in Matlab using FieldTrip [48] functions. Montecarlo cluster-based permutation dependent-samples t-test was applied to compare normalized PAC comodulograms (i. e. 2D matrix of all phase-amplitude frequency pairs) of the ASSR and rsEEG data for each algorithm (MVL-MI, KL-MI, PLV-MI) and frontocentral electrode (F1, Fz, F2, FC1, FCz, FC2, C1, Cz, C2) separately. 5000 permutations were performed. One-tailed test was selected to detect the positive clusters (higher PAC in ASSR vs rsEEG) with the alpha level at 0.05.

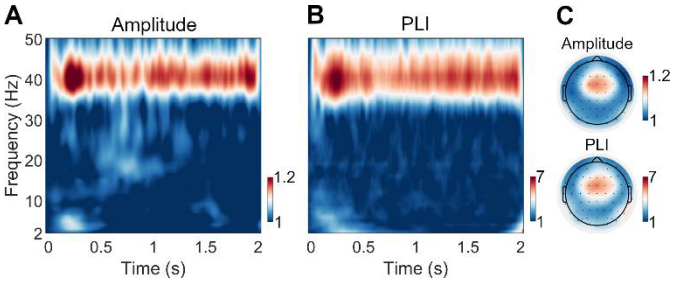

Fig. 3. ASSR data time-frequency plots depicting baseline-corrected amplitude (A), PLI (B) and topographic plots of amplitude and PLI averaged over 38-42 Hz and 500-2000 ms windows (C).

To assess potential differences in individual variation of PAC, for each subject, we extracted the phase-amplitude frequency pairs that showed the highest PAC value, further referred to as peak frequencies. Then, statistical evaluation of the peak frequencies was performed for each frontocentral electrode and PAC method separately. The PAC value of the peak frequencies (regardless of the frequencies themselves) was first compared between ASSR and rsEEG conditions using Wilcoxon Signed Rank test for repeated measures, assessing whether the magnitude of individual-specific maximum PAC value differs between conditions. Second, for the 2D matrix of peak frequencies, the centroid (X and Y coordinates representing mean phase and amplitude frequencies across subjects) was computed for ASSR and rsEEG conditions. For each subject, the Euclidean distance between the centroid and the subject-specific peak frequencies was derived. In order to test whether the spread of peak frequencies differed between conditions, Wilcoxon Signed Rank test was used to compare the distances from the centroid in ASSR and rsEEG data. Given the exploratory nature of the analysis, multiple comparisons correction was not applied.

III. Results

A. Time-Frequency Analysis

Time-frequency analysis was performed to assess the presence of ASSR in real EEG data. A clear 40-Hz ASSR was observed (Figure 3, A and B). As evident in topographic maps created for baseline-corrected amplitude and PLI by averaging over 38-42 Hz and 500-2000 ms windows (Figure 3C), ASSR was detected in the frontocentral area, thus the results for FCz channel are reported in detail. Mean baseline-normalized amplitude of ASSR (Figure 3A) was 1.15 ± 0.07, ranging from 1.05 to 1.3, while mean PLI (Figure 3B) was 5.57 ± 1.47 and the ranging 3.06-7.71. The results of the remaining channels are presented in the Supplementary material S2.

B. Phase-Amplitude Coupling

Simulated data. PAC was first computed on simulated data to demonstrate the capability of the analysis pipeline to detect PAC. Figure 4A presents PAC comodulograms for the simulated signal with imbedded coupling at 6/40 Hz - raw (non-normalized), surrogate (means of the surrogate distributions), and surrogate-normalized (z-score) PAC values are shown. MVL-MI and KL-MI generally showed a gradual

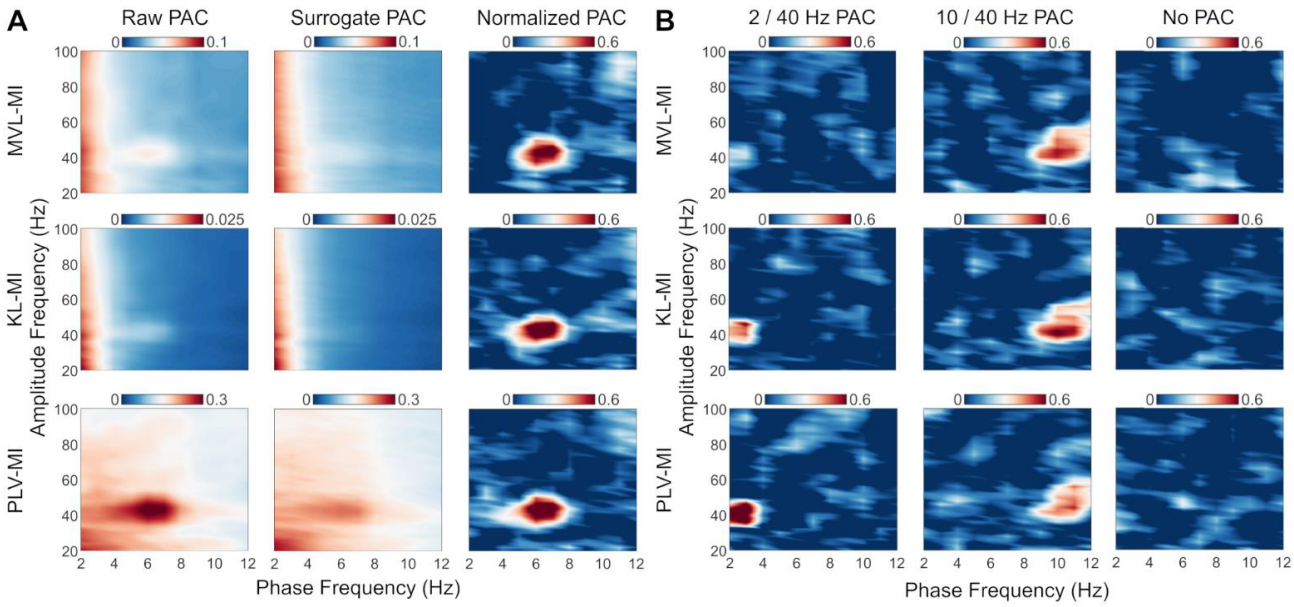

Fig. 4. Comodulograms showing PAC values in all phase-amplitude frequency pairs of simulated data. A depicts raw (non-normalized) PAC, mean PAC in the surrogate distributions and surrogate-normalized PAC in the signal with PAC simulated at 6/40 Hz phase/amplitude frequencies. B represents only normalized PAC in 2/40 Hz PAC, 10/40 Hz PAC and no-PAC signals.

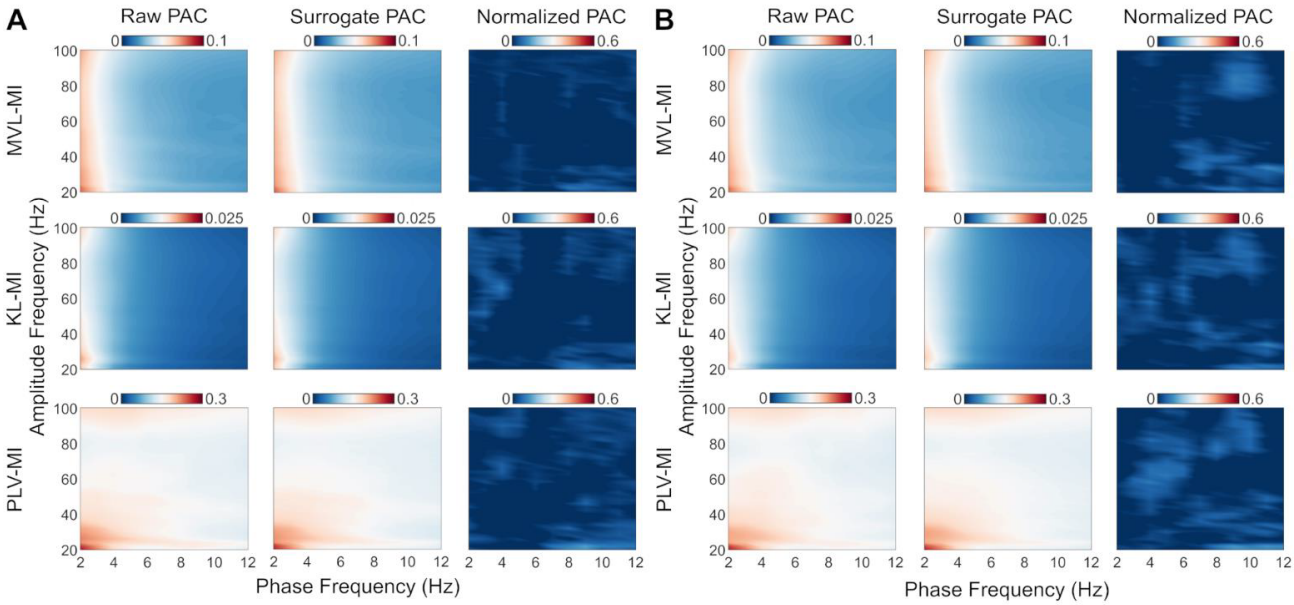

Fig. 5. PAC comodulograms of ASSR (A) and rsEEG (B) conditions, showing raw PAC (left), surrogate PAC (middle) and normalized PAC (right) for all analyzed phase-amplitude frequency pairs.

decline in raw PAC from lower to higher phase frequencies. At the amplitude frequency of 40 Hz, raw PAC estimated with MVL-MI was highest for delta (2-4 Hz; 0.064) frequencies, followed by theta (5-8 Hz; 0.047) and alpha (9-12 Hz; 0.027) frequencies; with KL-MI, raw PAC showed a similar trend (0.016, 0.007, 0.002). Conversely, PLV-MI showed stronger raw PAC at 40 Hz amplitude and theta phase frequencies (0.26) compared to other bands (delta - 0.23; alpha - 0.16). Surrogate PAC showed a similar pattern, but yielded lower values at theta (MVL-MI: 0.038; KL-MI: 0.005; PLV-MI: 0.21) phase frequencies compared to raw PAC. Accordingly, normalized z-score PAC showed clear peaks at simulated coupling frequencies: at 6/40 Hz (Figure 3A, right column), values were 0.57 (MVL-MI), 0.70 (KL-MI), and 0.62 (PLV-MI); at 2/40 Hz (Figure 3B, left column) values were 0.22, 0.40, and 0.64; and at 10/40 Hz (Figure 3B, middle column) values were 0.53, 0.62, and 0.42. When no PAC was introduced in the simulated signal (Figure 4B, right column), normalized PAC at 40-Hz amplitude and all phase frequencies did not exceed 0.19 for any estimation method.

Real EEG data. The grand average of raw, surrogate and normalized PAC of ASSR (A) and rsEEG (B) data at FCz are depicted in Figure 5. Comparison of ASSR and rsEEG normalized PAC comodulograms using cluster-based permutation test showed no significant clusters (cluster T-mass <32.95, cluster p >0.15) for any channel and method.

TABLE II
DESCRIPTIVE VARIABLES (MEANS AND SDS) OF PAC IN ASSR AND RSEEG DATA

		ASSR		rsEEG	
		Raw	Normalized	Raw	Normalized
MVL-MI	Delta	0.054 ± 0.002	-0.004 ± 0.04	0.053 ± 0.004	-0.029 ± 0.04
	Theta	0.029 ± 0.001	-0.024 ± 0.05	0.029 ± 0.002	0.029 ± 0.07
	Alpha	0.023 ± 0.002	-0.03 ± 0.08	0.023 ± 0.001	0.009 ± 0.049
KL-MI	Delta	0.01 ± 0.0004	-0.017 ± 0.06	0.01 ± 0.0006	0.016 ± 0.07
	Theta	0.004 ± 0.0002	-0.027 ± 0.04	0.004 ± 0.0002	0.015 ± 0.05
	Alpha	0.002 ± 0.0002	-0.026 ± 0.07	0.002 ± 0.0002	0.013 ± 0.05
PLV-MI	Delta	0.17 ± 0.01	-0.023 ± 0.06	0.17 ± 0.02	0.015 ± 0.09
	Theta	0.15 ± 0.007	-0.018 ± 0.06	0.16 ± 0.007	0.024 ± 0.06
	Alpha	0.14 ± 0.01	0.001 ± 0.08	0.14 ± 0.006	0.025 ± 0.06

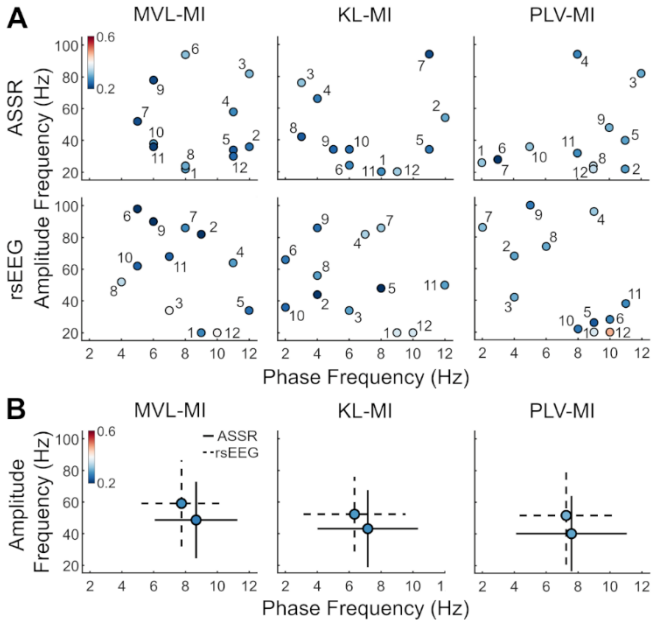

Fig. 6. Individual peak frequencies and their PAC values (A) and centroids (B) in ASSR and rsEEG conditions. Numbers near dots in A indicate subjects.

Table II presents average raw and normalized PAC values of ASSR and rsEEG data in delta (2-4 Hz), theta (5-8 Hz) and alpha (9-12 Hz) phase frequencies and 40-Hz amplitude frequency for each PAC estimation method. Qualitatively, very similar PAC patterns can be observed in both rsEEG and ASSR data. Similarly to simulated data, all methods (MVL-MI, KL-MI, PLV-MI) showed a general raw PAC decrease from lower to higher phase frequencies, while surrogate PAC mirrored these patterns. Z-normalized PAC did not reveal clear PAC peaks. At 40-Hz amplitude frequency, comparable normalized PAC values close to 0 were obtained in ASSR and rsEEG data and at all phase frequency bands using all methods.

Figure 6 illustrates individual-specific peak PAC frequency pairs (A) and centroids (B). When comparing max PAC values for each channel and extraction method, only one comparison reached statistical significance (MVL-MI, FC1 channel, z = -2.04, p = 0.04), with lower max PAC values observed in ASSR (0.24) than in rsEEG (0.29). Comparison of individual distances of PAC frequency pairs from the centroid resulted in a single statistically significant difference (KL-MI, Fz channel, z = 2.11, p = 0.03), showing a higher distance in ASSR data (27.8) compared to rsEEG (16.6). Descriptively, subject-specific peak frequencies (both in low and high range) showed high variability (Figure 6). In ASSR data, average of max PAC values was 0.27 ± 0.04 at peak frequencies of 8.7 ± 2.6 / 48.7 ± 24.2 Hz estimated with MVL-MI; 0.28 ± 0.04 at 7.2 ± 3.2 / 43.2 ± 24.4 Hz estimated with KL-MI; and 0.29 ± 0.04 at 7.6 ± 3.5 / 40.2 ± 23.8 Hz estimated with PLV-MI. In rsEEG data, average of max PAC value was 0.28 ± 0.07 at peak frequencies of 7.8 ± 2.5 / 59.2 ± 27.3 Hz estimated with MVL-MI; 0.29 ± 0.06 at 6.3 ± 3.2 / 52.3 ± 23.6 Hz estimated with KL-MI; and 0.31 ± 0.06 at 7.3 ± 2.9 / 51.7 ± 31.1 Hz estimated with PLV-MI.

IV. DISCUSSION

PAC is an emerging measure in EEG/MEG research that reflects cross-frequency interactions [10]. Studies have shown its potential for the application as a marker of brain activity changes in psychiatric conditions [18], [19], [20] or in relation to noninvasive brain stimulation [53], [54], [55]. Previous studies suggest that PAC could be probed using ASSR paradigm, with three works reporting significant stimulus-related PAC compared to the baseline no-stimulation period [33], [34], [37]. Other ASSR-PAC studies only compared PAC between clinical groups [31], [32] or between conditions [35], [36], showing mixed findings. All studies differed considerably in terms of the applied PAC estimation approaches and the extent to which confounding factors relevant to PAC were addressed [30]. Importantly, ASSR-PAC studies also provided a highly different level of detail in describing their analyses, obscuring the comparison of the outcomes. Due to these limitations, the presence of PAC during auditory periodic stimulation, despite preliminary evidence, remains an unresolved issue. Therefore, in this work, we aimed to perform a systematic analysis of PAC in the EEG data recorded during auditory steady-state stimulation and the resting-state. We sought to set up a rigorous PAC analysis pipeline, taking into consideration procedures recommended in PAC literature and addressing potential confounding factors of the widely-used PAC methods [30], listed in Table I. We addressed the recommendations regarding data length, preprocessing and analysis window selection alongside applied surrogate normalization with comparisons to resting state EEG outcomes and EEG-like simulated signal containing PAC.

The results of this work demonstrated that the selected analysis pipeline successfully detected PAC in the simulated signal, i.e. where PAC was actually present. The simulated data consisted of Brownian noise and an added periodic 40-Hz component with its amplitude modulated according to the phase of the lower-frequency activity naturally present in the generated Brownian signal. As a result, the simulated activity was inherently noisy, resembling typical EEG. This noise likely contributed to the emergence of spurious PAC at lower phase frequencies [51], particularly in the delta band, observable both in the raw and surrogate PAC results.

Moreover, the added 40-Hz component was contaminated by intrinsic 40-Hz fluctuations in the Brownian noise, likely leading to relatively low PAC values at the frequencies where true coupling was present when compared to spurious PAC magnitude. Nonetheless, surrogate normalization substantially improved the results by suppressing spurious PAC and enhancing the detection of genuine coupling. In addition, three PAC estimation methods - MVL-MI, KL-MI, PLV-MI - differed in their sensitivity to spurious coupling at delta phase frequencies in the presence of simulated delta/gamma PAC. The outcomes of MVL-MI were the most affected by spurious PAC even after normalization, whereas PLV-MI outcomes exhibited the lowest susceptibility during the detection of 2/40 Hz PAC. When estimating theta- and alpha-gamma PAC, the results of all three methods were comparable.

When real EEG data were analyzed using the same pipeline, raw and surrogate PAC showed a pattern of higher PAC values at lower phase frequencies, similarly to simulated data. However, surrogate normalization did not reveal consistent PAC in both ASSR and resting-state EEG data. In the latter condition, we did not expect to see specific patterns of PAC. Although studies suggest that PAC can be detected during the resting-state [16], averaging PAC values in regularly-spaced segments should not reveal significant PAC given that the resting-state activity is not time-locked. Conversely, we predicted that if stimulus-related PAC was present during 40-Hz periodic auditory stimulation, PAC should be reliably detected when averaging PAC estimates over epochs segmented based on the onset of auditory input. Yet, no significant differences in PAC between ASSR and resting-state conditions were revealed.

Previously, three studies reported significant PAC at auditory periodic stimulation frequency when compared to the inter-stimulus (baseline) period and the resting-state condition [33], [34], [37], demonstrating rather strong effect sizes. However, one of these studies did not describe the methodological approach in sufficient detail to allow for a proper evaluation/replication [37]. The remaining two studies differed substantially both in methodologies and reported findings. [33] analyzed source-level MEG data, applying surrogate normalization and conducting cluster-based permutation testing on PAC comodulograms to identify frequency pairs with significant stimulus-related PAC. Their analysis revealed PAC in response to 40-Hz stimulation, showing significant clusters at delta, theta, and alpha phase frequencies and amplitude frequencies around 40 Hz. PAC was observed in the right auditory cortex and only in a pooled sample of patients with schizophrenia and healthy controls. Notably, no significant stimulus-related PAC was found for 30-Hz stimulation. In contrast, [34] used sensor-level EEG data and analyzed non-normalized PAC averaged over specific frequency bands (theta phase: 4–6 Hz; gamma amplitude: 28–32 Hz) using 30-Hz auditory stimulation. Their results showed that in healthy controls, PAC during auditory stimulation was higher than during the baseline or resting-state period, particularly over the left frontocentral electrodes.

In this study we followed recommendations to address known PAC-related confounds: data length [38], filtering bandwidths [39], signal-to-noise ratio [40], edge artifacts [41], non-sinusoidal oscillations [42], non-stationary activity [39] and PAC output dependence on estimation method [38]. The direct comparison to previous works [33], [34] is complicated due to vast methodological differences in stimulation frequency, the use of surrogate normalization, and statistical comparison approach. We recognize several factors that may help explain the discrepancy in findings beyond the differences in the analyses pipelines. ASSRs generally show high phase consistency but the magnitude of the response measured with EEG is typically low [36], [56], [57]. This was confirmed in the time-frequency analysis of our EEG data showing low stimulus-related gamma amplitudes (on average, relative baseline-corrected value was 1.15), which may have constrained the detection of PAC-related amplitude fluctuations. In contrast, [33] analyzed data from 45 participants with response recorded using MEG, a modality that offers higher signal-to-noise ratio, sensitivity and spatial resolution than EEG [58], [59] for cortical sources, thus being better equipped to detect PAC associated with ASSR. Additionally, our results may have been affected by interindividual variability, which could have obscured consistent effects, particularly given the small sample size (see Supplementary Material S2). Notably, [33], [34] and [37] included larger cohorts and reported strong PAC effects. Our study sample size was based on the assumption, supported by prior literature, that PAC should be a robust and detectable outcome. Thus, while our sample size was sufficient to capture strong PAC effects, it did not provide adequate power to reliably detect small-to-moderate effects.

To further explore interindividual variability in ASSR data, we conducted the analysis of PAC at individual peak frequencies, which has not been previously applied in ASSR-PAC studies. We extracted the peak frequencies that exhibited the highest PAC values for each subject, aiming to assess individual variability. However, the peak frequencies varied substantially, without any systematic patterns (Figure 6). Additionally, neither the maximum PAC values nor the distribution of peak frequencies showed consistent differences between the ASSR and resting-state conditions. These results support the interpretation that periodic auditory stimulation did not elicit stimulus-related PAC. As discussed above, several factors may have reduced the sensitivity of our study to detect group-level PAC differences between the ASSR and resting-state conditions. Nevertheless, based on prior evidence [33], [34], [37], we expected that if PAC were reliably induced by periodic stimulation, it would at least be observable at a qualitative level in a subset of participants who demonstrated stable and robust ASSRs. However, this was not the case, as indicated by the stochastic spread of individual peak frequencies and the generally low peak PAC magnitudes (also, see Supplementary material S2 for time-frequency plots and PAC comodulograms of each subject).

Overall, the findings of this study challenge the idea that PAC occurs during the ASSR paradigm. Functionally, PAC is thought to facilitate the integration of local sensory information into broader perceptual or cognitive networks [60]. In the auditory domain, significant PAC has primarily been reported in relation to speech processing [11], [13], [14], [61], [62]. Mechanistically, an in silico study suggested that PAC can

arise in two scenarios: (1) due to external low-frequency input or (2) through interactions between two local oscillators with distinct frequencies [63]. Therefore, our results showing no significant PAC during auditory periodic stimulation are not surprising. ASSR is a passive, externally controlled oscillatory response at higher frequency bands, predominantly gamma, that mimics the pattern of the auditory stimulus [21] and maintains stability over time [24]. The stimuli used to evoke ASSRs are typically trains of brief, equally spaced noise clicks or amplitude-modulated sinusoidal tones that do not carry semantic or otherwise meaningful information. As such, the complex neural mechanisms necessary for PAC to occur may not be recruited in the processing of these simple stimuli.

Our study is the first one to systematically investigate the presence of PAC during auditory steady-state stimulation. Although we did not detect stimulus-specific PAC, further research is needed for a more definitive answer regarding the presence of PAC in relation to the ASSR paradigm. This would provide evidence whether auditory periodic stimulation is indeed useful for the purpose of PAC evaluation. We encourage future studies to incorporate PAC evaluation in their analysis of ASSR data, utilizing rigorous analysis approaches based on the recommendations outlined in PAC literature. Furthermore, alternative PAC methods could be used, e.g. Bayesian PAC [64], an approach based on generalized eigendecomposition [65] or event-related PAC [66], the latter of which could be particularly suitable for time-locked ASSR. Additionally, other types of cross-frequency interactions could be explored, e.g. phase-phase coupling [67]. Finally, future research would benefit from a comprehensive, in-depth exploration of PAC methodological aspects and the development of standardized, evidence-based analysis pipelines.

Acknowledgment

The authors thank Evaldas Pipinis and Vykinta Parčiauskaitė for help with data collection.

References

[1] G. Buzsaáki and A. Draguhn, "Neuronal oscillations in cortical networks," *Science*, vol. 304, no. 5679, pp. 1926–1929, Jun. 2004, doi: 10.1126/science.1099745.

[2] L. Meyer, "The neural oscillations of speech processing and language comprehension: State of the art and emerging mechanisms," *Eur. J. Neurosci.*, vol. 48, no. 7, pp. 2609–2621, Oct. 2018, doi: 10.1111/ejn.13748.

[3] C. E. Schroeder and P. Lakatos, "Low-frequency neuronal oscillations as instruments of sensory selection," *Trends Neurosciences*, vol. 32, no. 1, pp. 9–18, Jan. 2009, doi: 10.1016/j.tins.2008.09.012.

[4] L. M. Ward, "Synchronous neural oscillations and cognitive processes," *Trends Cognit. Sci.*, vol. 7, no. 12, pp. 553–559, Dec. 2003, doi: 10.1016/j.tics.2003.10.012.

[5] A. Hyafil, A.-L. Giraud, L. Fontolan, and B. Gutkin, "Neural cross-frequency coupling: Connecting architectures, mechanisms, and functions," *Trends Neurosciences*, vol. 38, no. 11, pp. 725–740, Nov. 2015, doi: 10.1016/j.tins.2015.09.001.

[6] O. Jensen and L. L. Colgin, "Cross-frequency coupling between neuronal oscillations," *Trends Cognit. Sci.*, vol. 11, no. 7, pp. 267–269, Jul. 2007, doi: 10.1016/j.tics.2007.05.003.

[7] B. Yakubov et al., "Cross-frequency coupling in psychiatric disorders: A systematic review," *Neurosci. Biobehavioral Rev.*, vol. 138, Jul. 2022, Art. no. 104690, doi: 10.1016/j.neubiorev.2022.104690.

[8] R. T. Canolty et al., "High gamma power is phase-locked to theta oscillations in human neocortex," *Science*, vol. 313, no. 5793, pp. 1626–1628, Sep. 2006, doi: 10.1126/science.1128115.

[9] A. B. L. Tort, R. Komorowski, H. Eichenbaum, and N. Kopell, "Measuring phase-amplitude coupling between neuronal oscillations of different frequencies," *J. Neurophysiol.*, vol. 104, no. 2, pp. 1195–1210, Aug. 2010, doi: 10.1152/jn.00106.2010.

[10] R. T. Canolty and R. T. Knight, "The functional role of cross-frequency coupling," *Trends Cognit. Sci.*, vol. 14, no. 11, pp. 506–515, Nov. 2010, doi: 10.1016/j.tics.2010.09.001.

[11] A. Borderie et al., "Cross-frequency coupling in cortico-hippocampal networks supports the maintenance of sequential auditory information in short-term memory," *PLOS Biol.*, vol. 22, no. 3, Mar. 2024, Art. no. e3002512, doi: 10.1371/journal.pbio.3002512.

[12] M. Köster, H. Finger, S. Graetz, M. Kater, and T. Gruber, "Theta-gamma coupling binds visual perceptual features in an associative memory task," *Sci. Rep.*, vol. 8, no. 1, p. 17688, Dec. 2018, doi: 10.1038/s41598-018-35812-7.

[13] M. Lizarazu, M. Carreiras, and N. Molinaro, "Theta-gamma phase-amplitude coupling in auditory cortex is modulated by language proficiency," *Hum. Brain Mapping*, vol. 44, no. 7, pp. 2862–2872, May 2023, doi: 10.1002/hbm.26250.

[14] M. Lizarazu, M. Lallier, and N. Molinaro, "Phase-amplitude coupling between theta and gamma oscillations adapts to speech rate," *Ann. New York Acad. Sci.*, vol. 1453, no. 1, pp. 140–152, Oct. 2019, doi: 10.1111/nyas.14099.

[15] B. Voytek, "Shifts in gamma phase-amplitude coupling frequency from theta to alpha over posterior cortex during visual tasks," *Frontiers Human Neurosci.*, vol. 4, Oct. 2010, Art. no. 191, doi: 10.3389/fnhum.2010.00191.

[16] E. Florin and S. Baillet, "The brain's resting-state activity is shaped by synchronized cross-frequency coupling of neural oscillations," *NeuroImage*, vol. 111, pp. 26–35, May 2015, doi: 10.1016/j.neuroimage.2015.01.054.

[17] M. Tanaka et al., "Magnetoencephalography detects phase-amplitude coupling in Parkinson's disease," *Sci. Rep.*, vol. 12, no. 1, p. 1835, Feb. 2022, doi: 10.1038/s41598-022-05901-9.

[18] J. I. Berman, S. Liu, L. Bloy, L. Blaskey, T. P. L. Roberts, and J. C. Edgar, "Alpha-to-gamma phase-amplitude coupling methods and application to autism spectrum disorder," *Brain Connectivity*, vol. 5, no. 2, pp. 80–90, Mar. 2015, doi: 10.1089/brain.2014.0242.

[19] C. de Hemptinne et al., "Exaggerated phase-amplitude coupling in the primary motor cortex in Parkinson disease," *Proc. Nat. Acad. Sci. USA*, vol. 110, no. 12, pp. 4780–4785, Mar. 2013, doi: 10.1073/pnas.1214546110.

[20] G. H. Won, J. W. Kim, T. Y. Choi, Y. S. Lee, K. J. Min, and K. H. Seol, "Theta-phase gamma-amplitude coupling as a neurophysiological marker in neuroleptic-naïve schizophrenia," *Psychiatry Res.*, vol. 260, pp. 406–411, Feb. 2018, doi: 10.1016/j.psychres.2017.12.021.

[21] C. A. Brenner et al., "Steady state responses: Electrophysiological assessment of sensory function in schizophrenia," *Schizophrenia Bull.*, vol. 35, no. 6, pp. 1065–1077, Nov. 2009, doi: 10.1093/schbul/sbp091.

[22] K. L. McFadden, S. E. Steinmetz, A. M. Carroll, S. T. Simon, A. Wallace, and D. C. Rojas, "Test-retest reliability of the 40 hz EEG auditory steady-state response," *PLoS ONE*, vol. 9, no. 1, Jan. 2014, Art. no. e85748, doi: 10.1371/journal.pone.0085748.

[23] B. J. Roach, D. C. D'Souza, J. M. Ford, and D. H. Mathalon, "Test-retest reliability of time-frequency measures of auditory steady-state responses in patients with schizophrenia and healthy controls," *NeuroImage, Clin.*, vol. 23, Jun. 2019, Art. no. 101878, doi: 10.1016/j.nicl.2019.101878.

[24] M. Van Eeckhoutte, R. Luke, J. Wouters, and T. Francart, "Stability of auditory steady state responses over time," *Ear Hearing*, vol. 39, no. 2, pp. 260–268, Mar. 2018, doi: 10.1097/aud.0000000000000483.

[25] O. H. Jefsen, Y. Shtyrov, K. M. Larsen, and M. J. Dietz, "The 40-Hz auditory steady-state response in bipolar disorder: A meta-analysis," *Clin. Neurophysiol.*, vol. 141, pp. 53–61, Sep. 2022, doi: 10.1016/j.clinph.2022.06.014.

[26] S. Sugiyama et al., "The auditory steady-state response: Electrophysiological index for sensory processing dysfunction in psychiatric disorders," *Frontiers Psychiatry*, vol. 12, Mar. 2021, Art. no. 644541, doi: 10.3389/fpsyt.2021.644541.

[27] M. Tada et al., "Differential alterations of auditory gamma oscillatory responses between pre-onset high-risk individuals and first-episode schizophrenia," *Cerebral Cortex*, vol. 26, no. 3, pp. 1027–1035, Mar. 2016, doi: 10.1093/cercor/bhu278.

[28] V. Parciauskaite, J. Bjekic, and I. Griskova-Bulanova, "Gamma-range auditory steady-state responses and cognitive performance: A systematic review," *Brain Sci.*, vol. 11, no. 2, p. 217, Feb. 2021, doi: 10.3390/brainsci11020217.

[29] G. Matulyte, V. Parciauskaite, J. Bjekic, E. Pipinis, and I. Griskova-Bulanova, "Gamma-band auditory steady-state response and attention: A systemic review," *Brain Sci.*, vol. 14, no. 9, p. 857, Aug. 2024, doi: 10.3390/brainsci14090857.

[30] A. Mockevičius and I. Griškova-Bulanova, "Phase-amplitude coupling during auditory steady-state stimulation: A methodological review," *Rev. Neurosciences*, vol. 36, no. 6, pp. 577–586, Feb. 2025, doi: 10.1515/revneuro-2024-0165.

[31] K. Kirihara, A. J. Rissling, N. R. Swerdlow, D. L. Braff, and G. A. Light, "Hierarchical organization of gamma and theta oscillatory dynamics in schizophrenia," *Biol. Psychiatry*, vol. 71, no. 10, pp. 873–880, May 2012, doi: 10.1016/j.biopsych.2012.01.016.

[32] V. Mancini et al., "Aberrant developmental patterns of gamma-band response and long-range communication disruption in youths with 22q11.2 deletion syndrome," *Amer. J. Psychiatry*, vol. 179, no. 3, pp. 204–215, Mar. 2022, doi: 10.1176/appi.ajp.2021.21020190.

[33] N. Murphy, N. Ramakrishnan, C. P. Walker, N. R. Polizzotto, and R. Y. Cho, "Intact auditory cortical cross-frequency coupling in early and chronic schizophrenia," *Frontiers Psychiatry*, vol. 11, p. 507, Jun. 2020, doi: 10.3389/fpsyt.2020.00507.

[34] W. Zhang et al., "Altered fronto-central theta-gamma coupling in major depressive disorder during auditory steady-state responses," *Clin. Neurophysiol.*, vol. 146, pp. 65–76, Feb. 2023, doi: 10.1016/j.clinph.2022.11.013.

[35] S. de la Salle et al., "Transcranial alternating current stimulation alters auditory steady-state oscillatory rhythms and their cross-frequency couplings," *Clin. EEG Neurosci.*, vol. 55, no. 3, pp. 329–339, May 2024, doi: 10.1177/15500594231179679.

[36] K. T. Jones, E. L. Johnson, Z. S. Tauxe, and D. C. Rojas, "Modulation of auditory gamma-band responses using transcranial electrical stimulation," *J. Neurophysiol.*, vol. 123, no. 6, pp. 2504–2514, Jun. 2020, doi: 10.1152/jn.00003.2020.

[37] R. Y. Cho et al., "Development of sensory gamma oscillations and cross-frequency coupling from childhood to early adulthood," *Cerebral Cortex*, vol. 25, no. 6, pp. 1509–1518, Jun. 2015, doi: 10.1093/cercor/bht341.

[38] M. J. Hülsemann, E. Naumann, and B. Rasch, "Quantification of phase-amplitude coupling in neuronal oscillations: Comparison of phase-locking value, mean vector length, modulation index, and generalized-linear-modeling-cross-frequency-coupling," *Frontiers Neurosci.*, vol. 13, Jun. 2019, Art. no. 573, doi: 10.3389/fnins.2019.00573.

[39] J. Aru et al., "Untangling cross-frequency coupling in neuroscience," *Current Opinion Neurobiol.*, vol. 31, pp. 51–61, Apr. 2015, doi: 10.1016/j.conb.2014.08.002.

[40] D. Dvorak and A. A. Fenton, "Toward a proper estimation of phase-amplitude coupling in neural oscillations," *J. Neurosci. Methods*, vol. 225, pp. 42–56, Mar. 2014, doi: 10.1016/j.jneumeth.2014.01.002.

[41] M. A. Kramer, A. B. L. Tort, and N. J. Kopell, "Sharp edge artifacts and spurious coupling in EEG frequency comodulation measures," *J. Neurosci. Methods*, vol. 170, no. 2, pp. 352–357, May 2008, doi: 10.1016/j.jneumeth.2008.01.020.

[42] D. Lozano-Soldevilla, N. ter Huurne, and R. Oostenveld, "Neuronal oscillations with non-sinusoidal morphology produce spurious phase-to-amplitude coupling and directionality," *Frontiers Comput. Neurosci.*, vol. 10, p. 87, Aug. 2016, doi: 10.3389/fncom.2016.00087.

[43] D. M. Groppe et al., "Dominant frequencies of resting human brain activity as measured by the electrocorticogram," *NeuroImage*, vol. 79, pp. 223–233, Oct. 2013, doi: 10.1016/j.neuroimage.2013.04.044.

[44] A. Mockevicius, J. Bjekic, and I. Griskova-Bulanova, "The modulation of steady-state responses by transcranial alternating current stimulation: A scoping review," *Front. Syst. Neurosci.*, vol. 19, 2025, Art. no. 1661128, doi: 10.3389/fnsys.2025.1661128.

[45] I. Griskova-Bulanova, K. Sveistyte, and J. Bjekic, "Neuromodulation of gamma-range auditory steady-state responses: A scoping review of brain stimulation studies," *Frontiers Syst. Neurosci.*, vol. 14, p. 41, Jun. 2020, doi: 10.3389/fnsys.2020.00041.

[46] A. Delorme and S. Makeig, "EEGLAB: An open source toolbox for analysis of single-trial EEG dynamics including independent component analysis," *J. Neurosci. Methods*, vol. 134, no. 1, pp. 9–21, Mar. 2004, doi: 10.1016/j.jneumeth.2003.10.009.

[47] H. Zhivomirov, "A method for colored noise generation," *Romanian J. Acoust. Vibrat.*, vol. 15, no. 1, Aug. 2018, Art. no. 1.

[48] R. Oostenveld, P. Fries, E. Maris, and J.-M. Schoffelen, "FieldTrip: Open source software for advanced analysis of MEG, EEG, and invasive electrophysiological data," *Comput. Intell. Neurosci.*, vol. 2011, Jul. 2011, Art. no. 156869, doi: 10.1155/2011/156869.

[49] R. A. Seymour, G. Rippon, and K. Kessler, "The detection of phase amplitude coupling during sensory processing," *Frontiers Neurosci.*, vol. 11, Sep. 2017, Art. no. 487, doi: 10.3389/fnins.2017.00487.

[50] F. Mormann et al., "Phase/amplitude reset and theta-gamma interaction in the human medial temporal lobe during a continuous word recognition memory task," *Hippocampus*, vol. 15, no. 7, pp. 890–900, Jan. 2005, doi: 10.1002/hipo.20117.

[51] E. Combrisson et al., "Tensorpac: An open-source Python toolbox for tensor-based phase-amplitude coupling measurement in electrophysiological brain signals," *PLOS Comput. Biol.*, vol. 16, no. 10, Oct. 2020, Art. no. e1008302, doi: 10.1371/journal.pcbi.1008302.

[52] F. Faul, E. Erdfelder, A.-G. Lang, and A. Buchner, "G*Power 3: A flexible statistical power analysis program for the social, behavioral, and biomedical sciences," *Behav. Res. Methods*, vol. 39, no. 2, pp. 175–191, May 2007, doi: 10.3758/bf03193146.

[53] S. Glim, Y. O. Okazaki, Y. Nakagawa, Y. Mizuno, T. Hanakawa, and K. Kitajo, "Phase-amplitude coupling of neural oscillations can be effectively probed with concurrent TMS-EEG," *Neural Plasticity*, vol. 2019, Mar. 2019, Art. no. 6263907, doi: 10.1155/2019/6263907.

[54] R. M. G. Reinhart and J. A. Nguyen, "Working memory revived in older adults by synchronizing rhythmic brain circuits," *Nature Neurosci.*, vol. 22, no. 5, pp. 820–827, May 2019, doi: 10.1038/s41593-019-0371-x.

[55] M. Mirjalili et al., "Individualized frequency and montage tACS to engage theta-gamma coupling and enhance working memory in mild cognitive impairment," *Frontiers Psychiatry*, vol. 16, Jun. 2025, Art. no. 1565881, doi: 10.3389/fpsyt.2025.1565881.

[56] V. Parciauskaite et al., "Individual resonant frequencies at low-gamma range and cognitive processing speed," *J. Personalized Med.*, vol. 11, no. 6, p. 453, May 2021, doi: 10.3390/jpm11060453.

[57] K. Takai et al., "Examining the role of novelty detection in 20- and 40-Hz auditory steady-state responses," *NeuroImage*, vol. 310, Apr. 2025, Art. no. 121136, doi: 10.1016/j.neuroimage.2025.121136.

[58] M. C. Piastra, A. Nüßing, J. Vorwerk, M. Clerc, C. Engwer, and C. H. Wolters, "A comprehensive study on electroencephalography and magnetoencephalography sensitivity to cortical and subcortical sources," *Hum. Brain Mapping*, vol. 42, no. 4, pp. 978–992, Mar. 2021, doi: 10.1002/hbm.25272.

[59] S. P. Singh, "Magnetoencephalography: Basic principles," *Ann. Indian Acad. Neurol.*, vol. 17, no. 1, pp. S107–112, Mar. 2014, doi: 10.4103/0972-2327.128676.

[60] M. Bonnefond, S. Kastner, and O. Jensen, "Communication between brain areas based on nested oscillations," *Eneuro*, vol. 4, no. 2, Mar. 2017, Art. no. ENEURO.0153-16.2017, doi: 10.1523/eneuro.0153-16.2017.

[61] A. Hyafil, L. Fontolan, C. Kabdebon, B. Gutkin, and A.-L. Giraud, "Speech encoding by coupled cortical theta and gamma oscillations," *eLife*, vol. 4, p. 06213, May 2015, doi: 10.7554/elife.06213.

[62] J. Wang, D. Gao, D. Li, A. S. Desroches, L. Liu, and X. Li, "Theta–gamma coupling reflects the interaction of bottom-up and top-down processes in speech perception in children," *NeuroImage*, vol. 102, pp. 637–645, Nov. 2014, doi: 10.1016/j.neuroimage.2014.08.030.

[63] Y. Qin, T. Menara, D. S. Bassett, and F. Pasqualetti, "Phase-amplitude coupling in neuronal oscillator networks," *Phys. Rev. Res.*, vol. 3, no. 2, Jun. 2021, Art. no. 023218, doi: 10.1103/physrevresearch.3.023218.

[64] D. Castillo-Barnes, A. Ortiz, P. Figueiredo, and N. J. Gallego-Molina, "A Bayesian framework for phase-amplitude cross-frequency coupling inference: Application to reading disability detection," *Expert Syst. Appl.*, vol. 291, Oct. 2025, Art. no. 128510, doi: 10.1016/j.eswa.2025.128510.

[65] M. X. Cohen, "Multivariate cross-frequency coupling via generalized eigendecomposition," *eLife*, vol. 6, p. 21792, Jan. 2017, doi: 10.7554/elife.21792.

[66] B. Voytek, M. D'Esposito, N. Crone, and R. T. Knight, "A method for event-related phase/amplitude coupling," *NeuroImage*, vol. 64, pp. 416–424, Jan. 2013, doi: 10.1016/j.neuroimage.2012.09.023.

[67] M. A. Belluscio, K. Mizuseki, R. Schmidt, R. Kempter, and G. Buzsáki, "Cross-frequency phase–phase coupling between theta and gamma oscillations in the hippocampus," *J. Neurosci.*, vol. 32, no. 2, pp. 423–435, Jan. 2012, doi: 10.1523/jneurosci.4122-11.2012.